Structural Rearrangements at Physiological pH: Nuclear Magnetic Resonance Insights from the V210I Human Prion Protein Mutant

ARTICLE *in* BIOCHEMISTRY · SEPTEMBER 2012

Impact Factor: 3.02 · DOI: 10.1021/bi3009856 · Source: PubMed

5 AUTHORS, INCLUDING:

Ivana Biljan
University of Zagreb
12 PUBLICATIONS **94** CITATIONS
SEE PROFILE

Gregor Ilc
National Institute of Chemistry
10 PUBLICATIONS **179** CITATIONS
SEE PROFILE

Gabriele Giachin
European Synchrotron Radiation Facility
27 PUBLICATIONS **233** CITATIONS
SEE PROFILE

Giuseppe Legname
Scuola Internazionale Superiore di Studi Avan…
184 PUBLICATIONS **6,195** CITATIONS
SEE PROFILE

BIOCHEMISTRY
including biophysical chemistry & molecular biology

Article

pubs.acs.org/biochemistry

Structural Rearrangements at Physiological pH: Nuclear Magnetic Resonance Insights from the V210I Human Prion Protein Mutant

Ivana Biljan,[†,@] Gregor Ilc,[†,‡] Gabriele Giachin,[§] Janez Plavec,*[,†,‡,∥] and Giuseppe Legname*[,§,⊥]

[†]Slovenian NMR Centre, National Institute of Chemistry, Hajdrihova 19, SI-1000 Ljubljana, Slovenia

[‡]EN→FIST Centre of Excellence, Dunajska 156, SI-1001 Ljubljana, Slovenia

[§]Laboratory of Prion Biology, Department of Neuroscience, Scuola Internazionale Superiore di Studi Avanzati (SISSA), via Bonomea 265, Trieste, Italy

[∥]Faculty of Chemistry and Chemical Technology, University of Ljubljana, Aškerčeva cesta 5, SI-1000 Ljubljana, Slovenia

[⊥]ELETTRA Laboratory, Sincrotrone Trieste S.C.p.A., I-34149 Basovizza, Trieste, Italy

ABSTRACT: A major focus in prion structural biology studies is unraveling the molecular mechanism leading to the structural conversion of PrP^{C} to its pathological form, PrP^{Sc}. In our recent studies, we attempted to understand the early events of the conformational changes leading to PrP^{Sc} using as investigative tools point mutations clustered in the open reading frame of the human PrP gene and linked to genetic forms of human prion diseases. In the work presented here, we investigate the effect of pH on the nuclear magnetic resonance (NMR) structure of recombinant human PrP (HuPrP) carrying the pathological V210I mutation responsible for familial Creutzfeldt-Jakob disease. The NMR structure of HuPrP(V210I) determined at pH 7.2 shows the same overall fold as the previously determined structure of HuPrP(V210I) at pH 5.5. It consists of a disordered N-terminal tail (residues 90−124) and a globular C-terminal domain (residues 125−231) comprising three α-helices and a short antiparallel β-sheet. Detailed comparison of three-dimensional structures of HuPrP(V210I) at pH 7.2 and 5.5 revealed significant local structural differences, with the most prominent pH-related structural variations clustered in the $\alpha_2-\alpha_3$ interhelical region, at the interface of the $\beta_1-\alpha_1$ loop, in helices α_1 and α_3, and in the $\beta_2-\alpha_2$ loop region. The detailed analysis of interactions among secondary structure elements suggests a higher degree of structural ordering of HuPrP(V210I) under neutral-pH conditions, thus implying that spontaneous misfolding of PrP^{C} may occur under acidic-pH conditions in endosomal compartments.

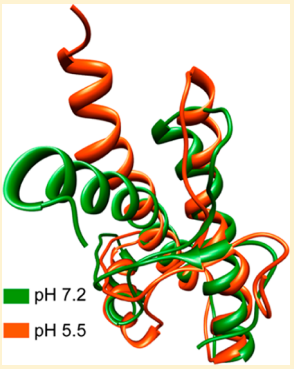

Transmissible spongiform encephalopathies (TSEs), or prion diseases, are invariably fatal neurodegenerative disorders affecting humans and animals. Human prion diseases include Creutzfeldt-Jakob disease (CJD), fatal familial insomnia (FFI), Gerstmann-Sträussler-Scheinker (GSS) syndrome, and kuru, whereas the most common prion diseases in animals are scrapie in sheep, bovine spongiform encephalopathy, and chronic wasting disease in cervids. Prion diseases are caused by misfolding of the physiological cellular prion protein, PrP^{C}, into a pathological form known as prion or PrP^{Sc}, which accumulates as amyloid in the brain of diseased individuals.[1] Most of the human prion diseases are sporadic, meaning that this event involves a stochastic refolding of PrP^{C} to its misfolded state. Approximately 10−15% of the cases are associated with mutations in the human (Hu) prion protein (PrP) gene (*PRNP*), and in very rare events, the etiologic agent can be acquired via an infectious route.

Structurally, PrP^{C} shares a very similar fold among different mammalian species.[2] It is a glycophosphatidylinositol (GPI)-anchored glycoprotein composed of 209 amino acids (in Hu numbering), including an N-terminal unstructured domain (residues 23−127) and a C-terminal globular domain.[3,4] The structured part features three α-helices and a short β-sheet. A single disulfide bond bridges helices α_2 and α_3. Similar to other GPI-anchored proteins, mature PrP^{C} is found attached to extracellular membrane domains rich in cholesterol and sphingolipids, also denoted as lipid rafts.[5] In contrast to that of PrP^{C}, the structure of PrP^{Sc} has significant β-sheet content (from 3 to 43%) and a decrease of α-helix content (from 42 to 30%).[6] The different structural features of PrP^{Sc} are responsible for the different biochemical properties of the two isoforms: while PrP^{C} is monomeric, soluble in nonionic detergents, and protease K-sensitive, PrP^{Sc} is insoluble, partially resistant to proteases, and prone to aggregation, thus making its structural characterization very difficult.[7]

A tilting point in prion biology is unraveling the molecular mechanism leading to the structural conversion of PrP^{C} to its pathological form, PrP^{Sc}. Several groups proposed that the neurotoxic signal triggered by PrP^{Sc} seems to be generated by an increased hydrophobic surface on the prion structure that allows intermolecular interactions and the accumulation of prion in neuronal cells.[8] In our recent studies, we tried to understand the early events of the conformational changes

Received: July 23, 2012
Revised: September 4, 2012
Published: September 4, 2012

dx.doi.org/10.1021/bi3009856 | *Biochemistry* 2012, 51, 7465−7474

Table 1. NMR Restraints and Structural Statistics for the Ensemble of the 20 Lowest-Energy Structures of HuPrP(90−231,M129,V210I) at pH 7.2

no. of NOE upper distance limits[a]	1929
intraresidual	452
sequential ($\|i - j\| = 1$)	480
medium-range ($\|i - j\| < 5$)	516
long-range ($\|i - j\| > 5$)	481
no. of torsion angle restraints	
backbone (φ and ψ)	158
rmsd from the mean coordinates (Å)	
ordered backbone atoms (residues 125−228)	0.81 ± 0.26
ordered heavy atoms (residues 125−228)	1.43 ± 0.21
Ramachandran plot (residues 125−231) (%)[b]	
residues in most favored regions	88.9
residues in additional allowed regions	10.2
residues in generously allowed regions	0.8
residues in disallowed regions	0.0
structure Z score[c]	
first-generation packing quality	−0.182 ± 0.668
second-generation packing quality	3.855 ± 1.533
Ramachandran plot appearance	−1.968 ± 0.266
χ_1/χ_2 rotamer normality	−4.321 ± 0.394
backbone conformation	−1.210 ± 0.202
rms Z score[c]	
bond lengths	1.147 ± 0.007
bond angles	0.497 ± 0.008
Ω angle restraints	0.619 ± 0.019
side chain planarity	0.951 ± 0.111
improper dihedral distribution	0.822 ± 0.027
inside/outside distribution	1.083 ± 0.016

[a]None of the 20 structures exhibits distance violations of >0.2 Å and torsion angle violations of >5°. [b]The ensemble of structures was analyzed by PROCHECK-NMR (version 3.4).[43] [c]The ensemble of structures was validated and analyzed using WhatIF.[44]

leading to PrP^{Sc} using as investigative tools point mutations clustered in *PRNP* and linked to genetic forms of human prion diseases. Comparing the nuclear magnetic resonance (NMR) structures of the wild-type (WT) HuPrP determined at acidic pH[4,9] with the NMR structures of Q212P[10] and V210I[11] HuPrP mutants linked to GSS and familial CJD (fCJD), respectively, allowed us to detect regions on HuPrP that may play a role during the early stage of the pathological conversion. These "hot spots" include an altered conformation of the $\beta_2-\alpha_2$ loop together with its increased spacing to the C-terminal end of helix α_3, a higher level of exposure of hydrophobic residues to solvent, and the narrowing of the angle between helices α_2 and α_3.

In the past few years, the use of PrP pathological mutants has emerged as an invaluable strategy for the comprehension of the molecular mechanisms leading to TSEs in transgenic (Tg) animal models.[12−16] Additionally, several studies investigated the role of pathological mutants in the context of protein misfolding and stability both in vitro and in silico.[17−19]

Another enigma in prion research is the identification of the subcellular site where pathogenic conversion takes place. It has been suggested that PrP^{C} misfolding and accumulation may occur during the endocytosis and internalization pathways.[20,21] Similar to other GPI-anchored proteins,[22] PrP^{C} is sequestered into intracellular endosomal compartments that are characterized by acidic pH values that can vary from pH 4.7 to 6.5.[23] Less information about the specific endosomes involved in prion conversion is available. Recent reports using cell culture models described PrP^{Sc} accumulation in both late[21] and recycling endosomes.[24] The latter are the likely sites of prion conversion. The accumulation of PrP^{Sc} in the endosomes and its secretion to the extracellular environment as multivesicular bodies formed within the endosomal system are thought to cause neuronal dysfunction and prion spreading.[25,26] Several biophysical and molecular dynamics (MD) studies indicated that the transition from the neutral to acidic pH regime induces substantial conformational changes and leads to rearrangements in the tertiary structure of PrP^{C}.[27−33] Interestingly, a high-resolution NMR structure of WT HuPrP at neutral pH pointed to only minor structural changes in comparison to the structure determined at pH 4.5.[33]

In this work, we aim to investigate the effect of pH on the structure of HuPrP carrying the pathological V210I mutation. The Val to Ile mutation at codon 210 is linked to fCJD,[34] and it is one of the most common mutations among inherited prion diseases in the European population.[35,36] The high-resolution three-dimensional (3D) structure of truncated recombinant HuPrP(90−231,M129,V210I) was determined at pH 7.2 by using solution-state NMR spectroscopy. Comparison of 3D structures of HuPrP(V210I) determined under conditions that mimic the environments of the cell surface (pH ∼7) and endosomal compartments (pH ∼4.7−6.5) revealed pH-related structural variations.

MATERIALS AND METHODS

Protein Expression and Purification. ^{13}C and ^{15}N doubly labeled HuPrP(90−231,M129,V210I) was expressed, purified, and refolded as previously described.[11] Briefly, the protein was

dx.doi.org/10.1021/bi3009856 | *Biochemistry* 2012, 51, 7465−7474

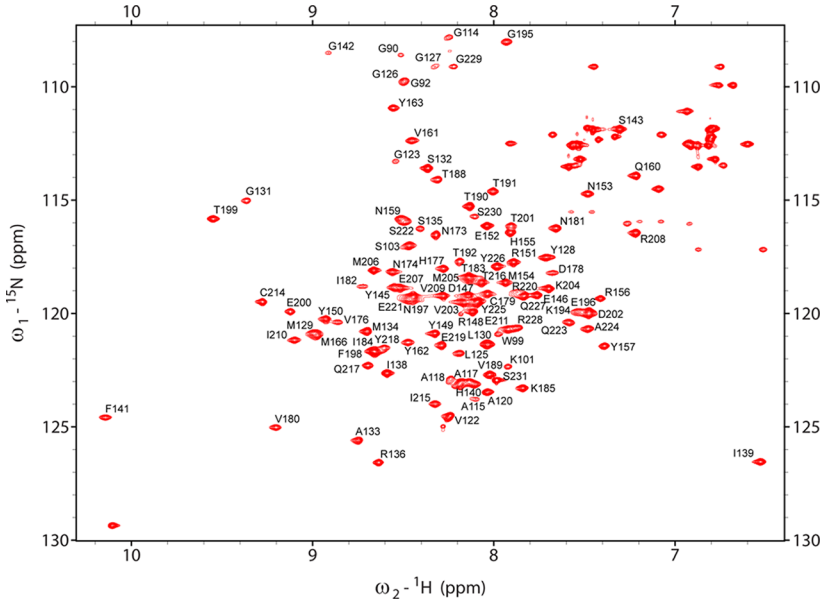

Figure 1. $^{1}H-^{15}N$ HSQC spectrum of HuPrP(V210I) at pH 7.2. Assigned backbone amide resonances are labeled using the one-letter amino acid code.

refolded under acidic conditions in a buffer solution containing 20 mM NaOAc and 0.005% NaN_3 (pH 5.5) and concentrated to 0.1 mM using centrifugal filter units (Amicrometer Ultra, Millipore). Subsequently, the protein was buffer-exchanged against 20 mM deuterated Tris, 20 mM KCl, and 0.005% NaN_3 (pH 7.2) using dialysis cassette devices (Thermo Scientific) and concentrated again to 0.8 mM.

NMR Spectroscopy. All NMR experiments were performed on ^{13}C and ^{15}N doubly labeled HuPrP(90−231,M129,V210I) protein on a Varian VNMRS 800 MHz NMR spectrometer using a ^{1}H, ^{13}C, ^{15}N triple-resonance probe-head with inverse detection at 298 K. NMR experiments with detection of HN were performed in a 90/10 H_2O/D_2O mixture at pH 7.2. HC-detected NMR data sets were acquired in 100% deuterated buffer. Standard triple-resonance NMR experiments were used for assignments and collection of distance restraints. Chemical shifts were referenced with respect to external 2,2-dimethyl-2-silapentane-5-sulfonic acid (DSS). All recorded spectra were processed with NMRPipe[37] and analyzed with Sparky[38] and CARA (available for free download from http://www.nmr.ch).[39]

Structure Calculations. The standard protocol of CYANA version 3.0 was used for automatic nuclear Overhauser effect (NOE) assignment and structure calculation.[40] The NOE assignment procedure[41] yielded 1929 distance restraints. The high-resolution 3D structure of V210I mutant was determined on the basis of 932 intraresidue and sequential, 516 medium-range, and 481 long-range distance constraints supported by 158 backbone torsion angle restraints (Table 1). The final cycle of CYANA calculation was started with 100 randomized conformers from which 20 conformers with the lowest residual target function values were used for additional refinement. Structure refinement was performed using the explicit solvent model in the YASARA program suite (http://www.yasara.org).[42] The refined ensemble of structures exhibited good convergence and very high definition. The validation procedure using PROCHECK-NMR[43] and WhatIF[44] demonstrated that the final ensemble of 3D structures is in agreement with the distance restraints and offers good geometry and side chain packing.

Data Deposition. The chemical shift data were deposited in Biological Magnetic Resonance Data Bank (entry 18550). The atomic coordinates were deposited in the Protein Data Bank (entry 2LV1).

RESULTS

Resonance Assignments. The $^{1}H-^{15}N$ HSQC NMR spectrum of HuPrP(V210I) at pH 7.2 (Figure 1) exhibits favorable chemical shift dispersion, indicating that the protein is correctly folded. Sequence-specific assignments of ^{1}H, ^{13}C, and ^{15}N backbone resonances were based on the following 3D NMR experiments: HNCO, HNCA, CBCA(CO)NH, and HNCACB. Assignments were additionally confirmed by inspection of sequential and medium-range NOEs in the 3D ^{15}N-edited NOESY-HSQC experiment. The H−N resonances of 119 of the 137 non-proline residues of HuPrP(V210I) were assigned. Fast exchange of amide protons with solvent at pH 7.2 prevented their observation for 12 amino acid residues from an unstructured N-terminal part (residues 90−124). No assignments could be obtained for the backbone amides of Arg164, Asp167, Tyr169, Ser170, Asn171, or Phe175. ^{1}H and ^{13}C resonances in aliphatic side chains were assigned with high completeness using 3D CC(CO)NH, (H)CCH-TOCSY, and ^{13}C-edited NOESY-HSQC experiments. Assignments of the side chain NH_2 groups of nine Asn and nine Gln residues by using 3D ^{15}N- and ^{13}C-edited NOESY-HSQC experiments were possible for seven Asn and six Gln residues. The remaining residues for which assignments could not be obtained were located in the flexible N-terminal part of HuPrP(V210I). Presumably, their side chain amide protons are involved in fast exchange with solvent at pH 7.2. ^{1}H and ^{13}C resonances in aromatic side chains of Tyr, Phe, His, and Trp residues were assigned on the basis of the analysis of the aromatic region of the 3D ^{13}C-edited NOESY-HSQC spectrum. δCH groups of His96, His111, and His187 and εCH groups of His96, His111, His155, His177, and His187 could not be

dx.doi.org/10.1021/bi3009856 | Biochemistry 2012, 51, 7465−7474

assigned because of the lack of NOEs between the imidazole ring protons and aliphatic protons of His residues. The Cys179−Cys214 disulfide bond was confirmed on the basis of Cβ chemical shifts of δ 40.9 and 42.0, respectively.[45] Peptide bonds in Xaa-Pro fragments adopt the *trans* conformation as indicated by their Cβ and Cγ chemical shifts and the corresponding cross-peaks in 3D ^{13}C-edited NOESY-HSQC spectra.

Solution Structure of HuPrP(V210I) at pH 7.2. The high-resolution 3D structure of HuPrP(V210I) at pH 7.2 was determined on the basis of 1929 NOE distance restraints obtained by analyzing 3D ^{15}N- and ^{13}C-edited NOESY-HSQC spectra. Additionally, the final structure calculation included 158 backbone torsion angle restraints. The 3D structure of HuPrP(V210I) at pH 7.2 is well-defined with average rmsd values of 0.81 Å for backbone atoms and 1.43 Å for heavy atoms (residues 125−228). Table 1 summarizes the complete structural statistics. The final ensemble of 20 NMR structures of HuPrP(V210I) is shown in Figure 2a.

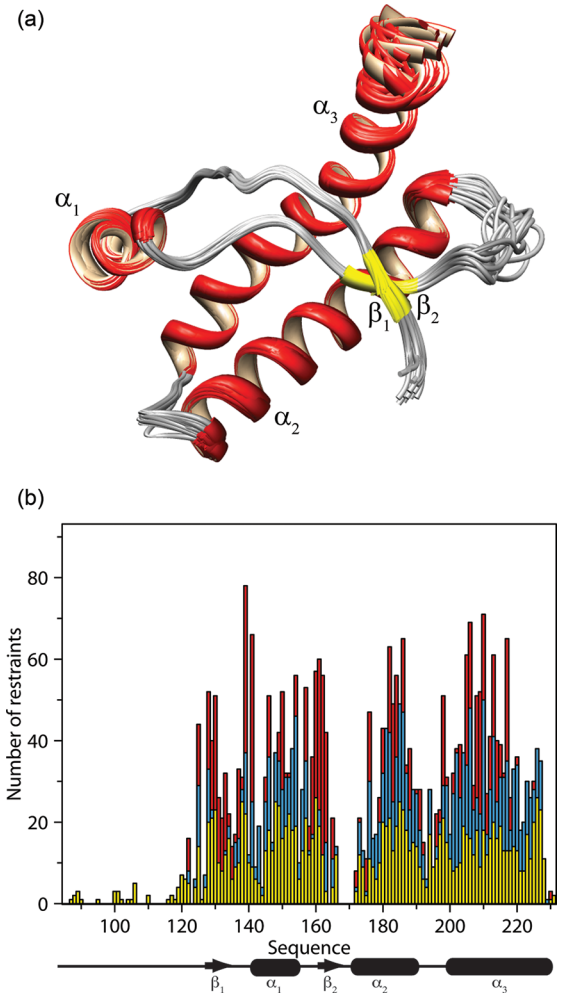

Figure 2. Overall 3D structure of HuPrP(V210I) at pH 7.2 and related NMR restraints. (a) Superposition of the 20 lowest-energy NMR structures of the folded domain (residues 125−228) of HuPrP(V210I). (b) Distribution of NOE restraints per residue. Intraresidual and sequential (yellow), medium-range (blue), and long-range (red) NOE contacts are presented. The five extra residues at the N-terminus are remnants of tobacco etch virus (TEV) cleavage.

The NMR solution-state structure of HuPrP(V210I) at pH 7.2 reveals an overall fold similar to those of other known PrP structures. It comprises an unstructured N-terminal part (residues 90−124) and a globular C-terminal domain (residues 125−231). The flexible tail at the N-terminus is characterized by a reduced number of observed backbone amide resonances as well as a small number of medium- and long-range NOE contacts (Figure 2b). The globular part contains three α-helices and one very short antiparallel β-sheet. A short helix α_1 spans residues 144−155, whereas antiparallel helices α_2 and α_3 contain residues 172−193 and 200−228, respectively. Helices α_2 and α_3 are connected through a short loop of residues 194−199 and further stabilized by a disulfide bond between Cys179 and Cys214. A short β-sheet is composed of two antiparallel β-strands comprising residues 129−131 (β_1) and 161−163 (β_2). The regions of the globular domain of HuPrP(V210I) exhibiting conformational variability include the loop connecting strand β_2 with helix α_2 (residues 164−171) and the C-terminal segment composed of residues 229−231. Backbone amide resonances for the several amino acid residues in the β_2−α_2 loop region could not be observed in the ^{1}H−^{15}N HSQC spectrum (vide supra). The origin of the missing cross-peaks may lie in conformational exchange processes on micro- to millisecond time scales leading to line broadening and reduction of cross-peak intensities. In addition, some structural disorder can be observed in the C-terminal part of helix α_3 (residues 218−228) as evidenced by a small number of long-range NOE contacts (Figure 2b). This segment of helix α_3 deviates from the helical axis defined by residues 200−217.

Stabilizing Interactions in HuPrP(V210I) at pH 7.2. The valine at codon 210 is part of a tightly packed 20-residue hydrophobic core responsible for the folding of helices α_2 and α_3 in the WT HuPrP.[46,47] It is one of the most solvent-protected amino acid residues in the PrP^C structure. To investigate the solvent accessibility of amino acid residues in HuPrP(V210I), we performed an NMR experiment in which protein was kept in deuterated buffer at neutral pH for several months. Under such an environment, the majority of amide protons were expected to exchange with deuterons, thus becoming NMR "invisible" in the proton frequency range. However, the backbone amide signals of several amino acid residues (Val180, Phe198, Met205, Ile210, Cys214, Ile215, Gln217, and Tyr218) could still be detected in ^{1}H−^{15}N HSQC spectra after 3 months (Figure 3a), indicating that they form a well-protected, solvent-inaccessible region of the structure of HuPrP(V210I).

The tertiary structure of HuPrP(V210I) is stabilized by a network of hydrophobic interactions between residues from helices α_2 and α_3 and between residues situated at the interfaces of the β_1−α_1 loop, helix α_1, the α_1−β_2 loop, and helix α_3. The hydrophobic core at the interface of helices α_2 and α_3 involves the following residues: Phe175, Val176, Cys179, Val180, Thr183, Ile184, and Thr188 from helix α_2 and Val203, Met206, Ile210, Met213, Cys214, Ile215, and Tyr218 from helix α_3 (Figure 3b). Close contacts between antiparallel helices α_2 and α_3 are defined by 81 experimentally observed long-range NOEs. Mutation of Val to Ile at codon 210 introduces steric hindrance into the interhelical α_2−α_3 region because of the bulkier Ile side chain.[11] As a result, the side chains of several residues, which are in direct contact with Ile210 (e.g., Ile184) or involved in hydrophobic interactions with other residues within the α_2−α_3 interhelical interface (e.g., Phe175 and Ile215), change their orientation. Nevertheless, the majority of

dx.doi.org/10.1021/bi3009856 | *Biochemistry* 2012, 51, 7465−7474

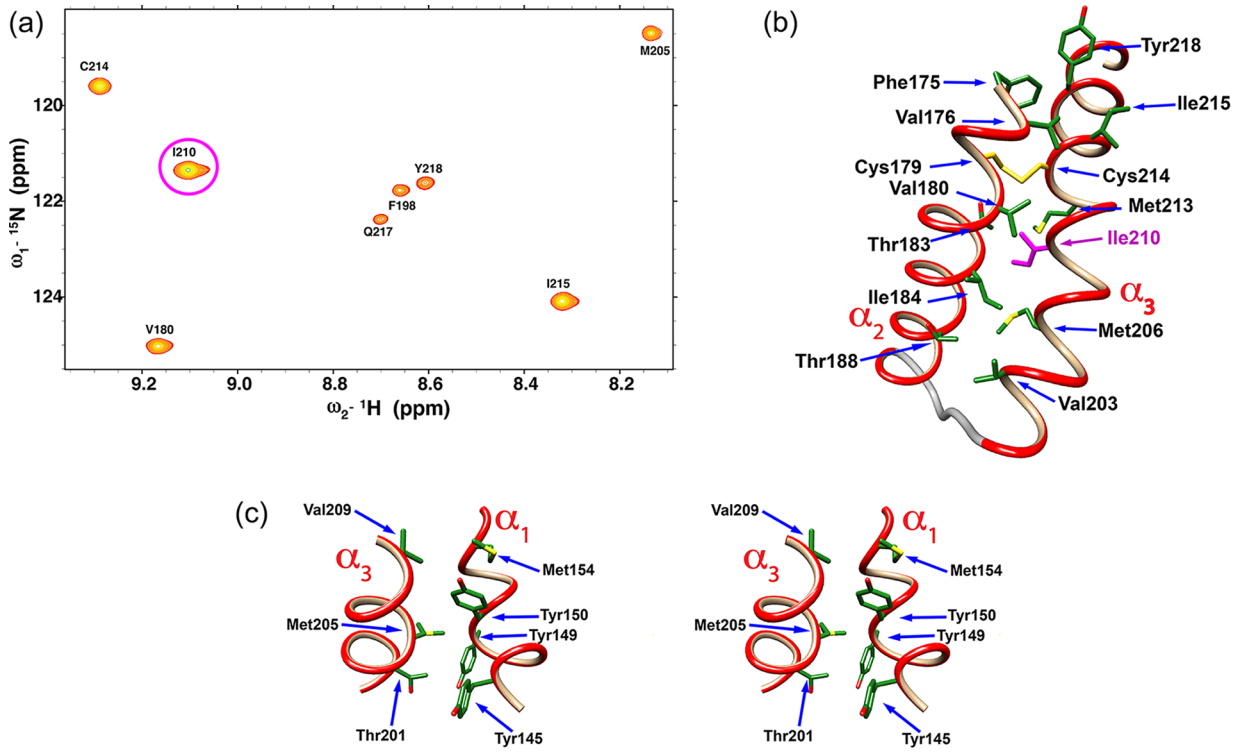

Figure 3. Hydrophobic features and interactions between helices in HuPrP(V210I) at pH 7.2. (a) $^{1}H-^{15}N$ HSQC spectrum of HuPrP(V210I) acquired after 3 months at pH 7.2 in deuterated buffer. Backbone amide resonances of residues protected from exchange with solvent deuterium are labeled using the one-letter amino acid code. The cross-peak corresponding to Ile210 is labeled with a magenta circle. (b) Hydrophobic interactions among hydrophobic residues at the interface of helices α_2 and α_3. The mutated residue Ile210 is colored magenta. Helices α_2 and α_3 are connected by the Cys179−Cys214 disulfide bridge (yellow). (c) Stereoview of hydrophobic interactions at the $\alpha_1-\alpha_3$ interhelical interface.

stabilizing interactions within the interhelical $\alpha_2-\alpha_3$ region in HuPrP(V210I) are conserved with respect to the WT protein. Ile210 itself is involved in hydrophobic interactions with Val180, Thr183, and Ile184 from helix α_2 and Met206 from helix α_3 (Figure 3b).

The globular domain of HuPrP(V210I) is further stabilized by the tight packing between helices α_1 and α_3 favored by hydrophobic contacts of Tyr145, Tyr149, Tyr150, and Met154 from helix α_1 and Thr201, Met205, and Val 209 from helix α_3 (Figure 3c). Tyr145, Tyr150, and Met154 from helix α_1 and Met205 and Val209 from helix α_3 are also involved in hydrophobic interactions with Pro137, Ile138, Ile139, and Phe141 from the $\beta_1-\alpha_1$ loop. Moreover, Tyr150 and Met154 from helix α_1 are engaged in hydrophobic contacts with Tyr157 from the $\alpha_1-\beta_2$ loop.

In addition to hydrophobic interactions, salt bridges and hydrogen bonds also play an important role in contributing to the structural stability of HuPrP(V210I). Several salt bridges and hydrogen bonds were identified within helices $\alpha_1-\alpha_3$ in the majority of structures from the final NMR ensemble. In helix α_1, Asp147 is involved in a salt bridge interaction with Arg151. There is also a salt bridge between Arg156 and Glu196 that orients the C-terminal end of helix α_1 toward the $\alpha_2-\alpha_3$ loop. A number of side chain−backbone hydrogen bonds are present within helix α_2. Thus, the side chain of Asn181 is involved in hydrogen bond interactions with carbonyl groups of His177 and Asp178. The side chains of Thr183, Thr188, Thr191, Thr192, and Thr193 form hydrogen bonds with the carbonyl groups of Cys179, Ile184, His187, Thr188, and Val189, respectively. Helix α_3 is stabilized by a hydrogen bond between the side chains of Thr199 and Asp202 and between the side chain of Thr216 and the carbonyl group of Gln212. In addition, the side chains of Gln217 and Arg220 from helix α_3 are involved in long-range hydrogen bond interactions with the carbonyl group of Ser132 from the $\beta_1-\alpha_1$ loop, presumably leading to the tilt of helix α_3 toward the $\beta_1-\alpha_1$ loop.

Effect of pH on the Tertiary Structure of HuPrP(V210I). An overlay of the $^{1}H-^{15}N$ HSQC NMR spectra of HuPrP(V210I) at pH 5.5 and 7.2 is shown in Figure 4a. Detailed analysis of $^{1}H-^{15}N$ HSQC spectra revealed that chemical shifts for the majority of amide resonances observed do not differ substantially at pH 5.5 and 7.2. This indicates that the overall structure of HuPrP(V210I) remains unperturbed with a change in pH. However, some of the backbone amide resonances are affected by an increase in pH from 5.5 to 7.2, suggesting pH-induced structural rearrangements (Figure 4a). Significant alterations in chemical shifts of ^{1}H and ^{15}N backbone resonances are mainly localized at helical regions of HuPrP(V210I), in particular helix α_2, and at the residues from the $\beta_1-\alpha_1$ and $\alpha_2-\alpha_3$ loops.

Next, we compared the $^{13}C\alpha$ chemical shifts of HuPrP(V210I) at pH 7.2 and 5.5 (Figure 4b). The most pronounced $^{13}C\alpha$ chemical shift differences ($\Delta\delta > 0.5$ ppm) were observed for His140 from the $\beta_1-\alpha_1$ loop and for residues 187−193 from helix α_2. The pronounced downfield chemical shift changes of $^{13}C\alpha$ of these residues indicate an increase in helical content at pH 7.2 in comparison to that at pH 5.5. Tyr163 from strand β_2, His177 from helix α_2, and Thr216 from helix α_3 also display significant $^{13}C\alpha$ chemical shift differences ($\Delta\delta > 0.3$ ppm in Figure 4b). A superposition of the 3D structures of folded regions (residues 125−228) of HuPrP(V210I) at pH 5.5 and 7.2 revealed that their backbone atoms can be super-

dx.doi.org/10.1021/bi3009856 | *Biochemistry* 2012, 51, 7465−7474

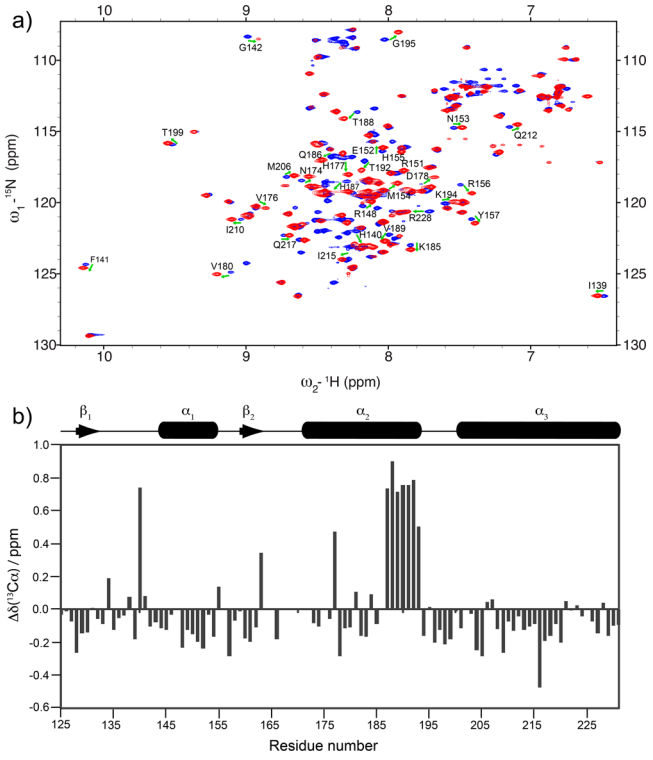

Figure 4. pH-induced changes in backbone ^{1}H, ^{15}N, and $^{13}C\alpha$ resonances in HuPrP(V210I). (a) Overlay of ^{1}H–^{15}N HSQC spectra of HuPrP(V210I) acquired at pH 5.5 (blue) and pH 7.2 (red). Residues displaying the most pronounced changes in the chemical shifts of ^{1}H and ^{15}N backbone resonances are indicated with one-letter amino acid codes. (b) $^{13}C\alpha$ chemical shift differences, $\Delta\delta(^{13}C\alpha) = \delta(\text{pH } 7.2) - \delta(\text{pH } 5.5)$ in HuPrP(V210I), as a function of residue number.

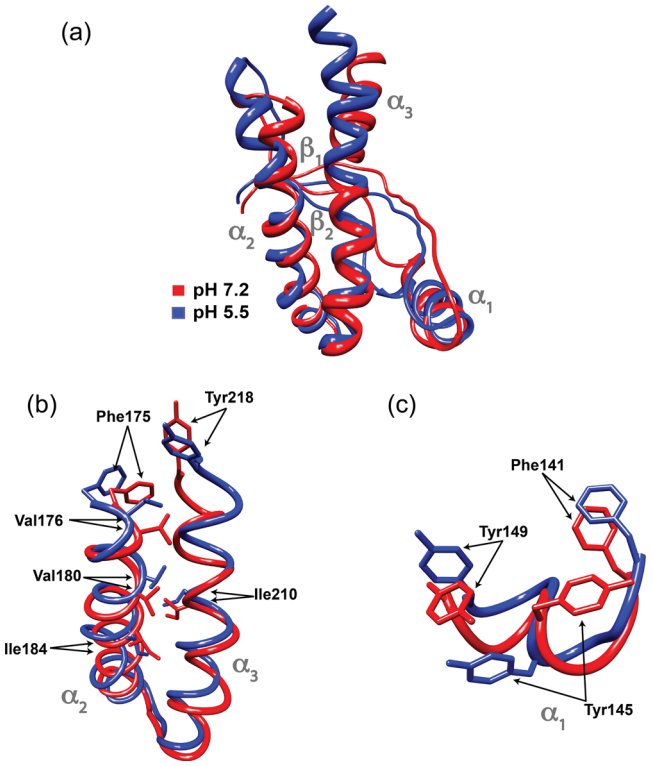

Figure 5. Comparison of HuPrP(V210I) structures at pH 7.2 and 5.5. (a) Overlay of the backbone heavy atoms of folded domains (residues 125–228) at pH 7.2 (red, PDB entry 2LV1) and pH 5.5 (blue, PDB entry 2LEJ). (b) Hydrophobic interactions between helices α_2 and α_3. (c) π–π interactions at the interface of the β_1–α_1 loop and helix α_1.

imposed with an rmsd of 1.42 Å (Figure 5a). Although both structures share a similar global architecture, careful inspection revealed a number of local pH-induced structural alterations. The hydrophobic interface of helices α_2 and α_3 is one of the regions in the globular domain of HuPrP(V210I) being affected by the change in pH (Figure 5b). Interactions between helices α_2 and α_3 form a part of the hydrophobic core of HuPrP(V210I) and are therefore important for maintaining the overall stability of the globular domain of HuPrP. As evidenced by the HuPrP(V210I) structures at both pH 5.5 and 7.2, the mutation of Val to bulkier Ile induces some rearrangements in the α_2–α_3 region. Whereas at pH 5.5 such rearrangements lead to loosening of several hydrophobic contacts at the α_2–α_3 interhelical interface, at pH 7.2 the majority of hydrophobic interactions are maintained. The differences are manifested through shorter inter-residue Val176–Val180, Val180–Ile184, and Phe175–Tyr218 distances at pH 7.2 than at pH 5.5 (Table 2). More pronounced interhelical α_2–α_3 interactions at pH 7.2 in comparison to pH 5.5 are directly supported by a higher number of long-range NOE contacts (81 at pH 7.2 vs 56 at pH 5.5).

Local structural variations between the 3D structures of HuPrP(V210I) under two different pH conditions can also be observed at the interface of the β_1–α_1 loop and helices α_1 and α_3. At pH 7.2, Tyr145 from helix α_1 is involved in π–π stacking interactions with Phe141 from the β_1–α_1 loop and Tyr149 from helix α_1 (Figure 5c). These three aromatic residues form a hydrophobic cluster. On the other hand, at pH 5.5 the side chain of Tyr145 adopts a different orientation and the Phe141–Tyr145–Tyr149 hydrophobic cluster is not present. The loss of π–π interactions is illustrated by substantially prolonged Phe141–Tyr145 and Tyr145–Tyr149 distances (Table 2) with respect to those in HuPrP(V210I) at pH 7.2. The change in orientation of the side chain of Tyr145 at pH 7.2 allows it to interact with residues from helix α_3, e.g., Met205. The contacts at the α_1–α_3 interhelical interface in HuPrP(V210I) at pH 7.2 are strengthened through long-range hydrophobic forces between Met154 from helix α_1 and Val209 from helix α_3. Noteworthy is the fact that Tyr145–Met205 and Met154–Val209 hydrophobic interactions are not present in HuPrP-(V210I) at pH 5.5.

In addition to hydrophobic interactions, the change in pH also affected interactions of polar amino acid residues in HuPrP(V210I). The globular domain contains the following four His residues: His140, His155, His177, and His187. At pH 5.5, the salt bridge interaction of His140 with Asp147 was detected in four of the 20 final NMR structures of HuPrP(V210I). In contrast, the His140–Asp147 salt bridge is not present in any of the structures at pH 7.2. The salt bridge between His177 and Glu211 was found in three structures from the final ensemble at pH 5.5 and in none at pH 7.2. The side chains of His155 and His187 are not involved in any salt bridge interactions at pH 5.5 or 7.2.

DISCUSSION

A hallmark of prion diseases is the conformational conversion of PrP^C into a disease-associated form, PrP^{Sc}. PrP^{Sc} self-propagates by inducing abnormal folding of PrP^C, subsequently

dx.doi.org/10.1021/bi3009856 | *Biochemistry* 2012, 51, 7465–7474

Table 2. Distances between Residues in the Structures of HuPrP(V210I) at pH 7.2 and 5.5[a]

	V176($C\gamma_1$)–I180($C\gamma_2$)	V180($C\gamma_1$)–I184($C\beta$)	F175($C\zeta$)–Y218($C\delta_2$)	F141($C\beta$)–Y145($C\varepsilon_2$)	Y145($C\beta$)–Y149($C\varepsilon_1$)	Y163($C\zeta$)–Y218($C\delta_2$)	Y163($C\zeta$)–F175($C\zeta$)
pH 7.2[b]	4.3 ± 0.1	5.2 ± 0.1	4.9 ± 0.3	3.9 ± 0.1	3.7 ± 0.1	7.5 ± 0.5	4.8 ± 0.5
pH 5.5[c]	7.7 ± 0.2	8.4 ± 0.1	8.4 ± 0.4	10.7 ± 0.6	9.3 ± 0.2	14.9 ± 0.3	7.7 ± 0.4

[a]The average distances and standard deviations in angstroms were calculated for the ensemble of 20 structures. [b]PDB entry 2LV1. [c]PDB entry 2LEJ.

leading to aggregation and brain damage. Recent studies suggest that the causative agents of many neurodegenerative illnesses affecting humans, including Alzheimer's disease and Parkinson's disease, are in fact prions.[48] The prion-like behavior of proteins causing these neurodegenerative disorders provides an explanation for the late onset of the diseases and, most importantly, offers new clues for the development of effective therapeutics. The necessary prerequisite to prevent and treat these neurodegenerative diseases is to know where and how formation of prions occurs. Earlier studies have indicated that the decrease in pH could trigger the conformational transition of PrP^C to PrP^{Sc}.[27−30,32] Apparently, HuPrP undergoes conformational rearrangements already under mildly acidic conditions in the pH range from 4.4 to 6.[31] These findings suggest that among the two proposed sites of PrP^C misfolding, on the cell surface where the pH is around 7 or in the endosomal compartments where the pH is between 4.7 and 6.5, the latter seems more likely. However, there is a lack of experimental high-resolution information about structural features of PrP^C under pH conditions mimicking the environments of the cell surface and endosomes. Here, we addressed this issue by determining the high-resolution 3D structure of the HuPrP carrying the fCJD-related V210I mutation at pH 7.2 and comparing it with the recently determined NMR structure determined under mildly acidic pH conditions.[11] The comparison demonstrated that change in pH from 5.5 to 7.2 did not affect the global architecture of HuPrP(V210I). Nonetheless, careful inspection revealed that 3D structures of HuPrP(V210I) at pH 5.5 and 7.2 display significant local structural differences. The most prominent pH-related changes involve the alterations in interactions within the hydrophobic core of HuPrP(V210I). At pH 5.5, several hydrophobic contacts between residues from helices α_2 and α_3 are lost. Moreover, at pH 7.2 in comparison to pH 5.5, HuPrP(V210) exhibits more compact packing of hydrophobic residues at the interface of the β_1−α_1 loop and helices α_1 and α_3. Additional stabilization at the interface of these secondary structure elements at pH 7.2 is provided through hydrophobic contacts between Phe141 and Tyr145, Tyr145 and Tyr149, Tyr145 and Met209, and Met154 and Val209, which are not present at pH 5.5. In addition to electrostatic interactions that stabilize the highly hydrophilic part of helix α_1 (e.g., Asp147−Glu151 salt bridge), hydrophobic interactions are very important for maintaining the stability of helix α_1 and for its interactions with other parts of the globular domain of HuPrP. In this regard, it is interesting to note that helix α_1 was proposed as a facilitator of PrP^C aggregation.[49,50] These studies suggested that the separation of the β_1−α_1 loop, helix α_1, and the α_1−β_2 loop from the α_2−α_3 region is required during the early stages of the conversion process. In addition, MD studies highlighted the role of helix α_1 in the early steps of PrP^C misfolding induced by a decrease in pH.[27,28,32] According to MD simulations, lowering the pH induces a loss of contacts between helix α_1 and other secondary structure elements in the globular domain of PrP^C. As a result, the hydrophobic core becomes unstable and helix α_1 and the preceding β_1−α_1 loop are displaced from the rest of the globular domain. Our structural data at two pH values suggest that the weakening of interactions at the interface of the β_1−α_1 loop, in helices α_1 and α_3, and between helices α_2 and α_3 in HuPrP(V210I) occurs under mildly acidic pH conditions (pH 5.5).

Another interesting point is the increase in the α-helical content according to downfield chemical shift changes observed for the segment of helix α_2 comprising residues 187−193 at pH 7.2. The similar features were observed in the NMR solution-state structures of WT HuPrP at different pH values.[33] It has been suggested that local destructuring of the C-terminal part of helix α_2 under acidic-pH conditions occurs because of the positive charge on His187 allowing the formation of the His187−Glu196 salt bridge.[30,32,33,51] The destabilizing effect of the positive charge in the C-terminal part of helix α_2 is correlated with the existence of several disease-linked mutations that introduce positive charges in this region (e.g., H187R, T188R/K, E200K, and D202N). In HuPrP(V210I) at pH 5.5, His140 and His177 form salt bridges with Asp147 and Glu211, respectively, whereas no salt bridge interactions could be detected for His155 and His187. On the other hand, none of the His residues is involved in salt bridge interactions at pH 7.2. Formation of a salt bridge between His140 and Asp147 at pH 5.5 could be responsible for the displacement of the side chain of Tyr145 with respect to its position in HuPrP(V210I) at pH 7.2. As a consequence, aromatic interactions of Tyr145 with Phe141 and Tyr149 that are present at pH 7.2 are lost at pH 5.5. Presumably, all His residues are mainly unprotonated at pH 7.2. Significant protonation of His155 and His187 is expected only below pH 5.5.[51] The partial protonation of these two His residues cannot be excluded under mildly acidic conditions as indicated by the distribution of electrostatic surface potential at pH 7.2 with respect to that at pH 5.5. The surface of HuPrP(V210I) is characterized by larger areas of positive charge under mildly acidic pH conditions with respect to neutral pH. Variations in charge distribution at pH 7.2 and 5.5 are mainly clustered around four His residues, from predominantly neutral to positive charge, respectively (Figure 6). The NMR structure of WT HuPrP at neutral pH[33] and MD simulations[51] indicated that His140 and His155 are involved in hydrogen bond interactions with Asp147 and Arg156, respectively. In addition, the same MD study pointed to formation of a His187−Arg156 hydrogen bond. None of these interactions were detected in the NMR structure of HuPrP-(V210I) at pH 7.2.

Structural findings reported in our recent work on HuPrP-(V210I) at pH 5.5[11] indicated that in addition to rearrangements within the hydrophobic α_2−α_3 interhelical interface, mutation of valine to isoleucine at codon 210 alters the conformation of the β_2−α_2 loop and increases the distance between this loop and helix α_3 with respect to that of WT HuPrP.[11] Subsequently, this conformational rearrangement results in a higher level of exposure of hydrophobic residues to solvent. In turn, intermolecular interactions involved in

dx.doi.org/10.1021/bi3009856 | Biochemistry 2012, 51, 7465−7474

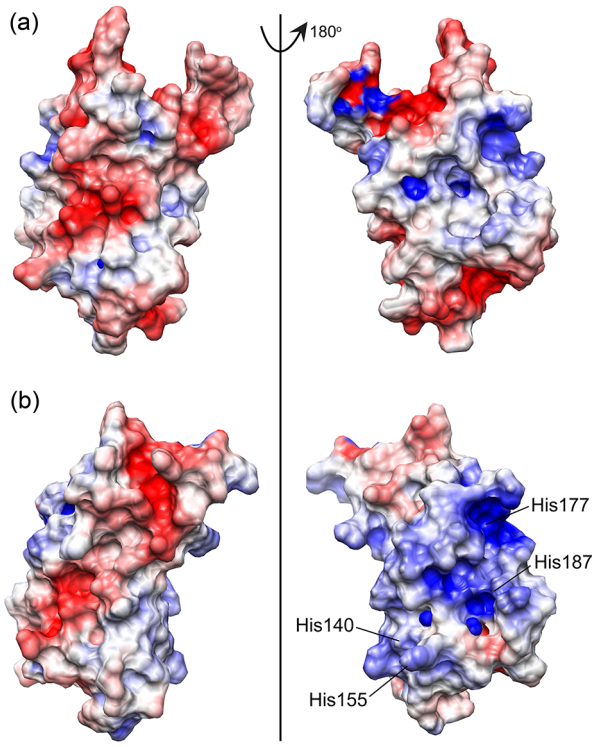

Figure 6. Electrostatic surface potential in HuPrP(V210I) at (a) pH 7.2 and (b) pH 5.5 viewed in the same orientations (left) as in Figure 5a and rotated by 180° around the vertical axis (right). Regions of negative and positive electrostatic potential are colored red and blue, respectively. The potentials were calculated with PDB2PQR,[52] APBS,[53] and PROPKA.[54]

spontaneous formation of PrP^{Sc} may be facilitated in inherited prion diseases. The $\beta_2-\alpha_2$ loop region demonstrates similar structural features in HuPrP(V210I) at both pH 5.5 and 7.2. The aromatic ring of Tyr169, at the center of the loop, is exposed to solvent. Consequently, there are no close contacts with the nearby aromatic residues such as Tyr163, Phe175, and Tyr218 at either pH value (Figure 7). In HuPrP(V210I) at pH 5.5, orientations of the side chains of Tyr163 and Phe175 are changed, leading to loss of their mutual contacts and long-range $\pi-\pi$ interactions with Tyr218 from helix α_3 that are present at higher pH. Unlike at acidic pH, at pH 7.2 shorter distances among Tyr163–Phe175, Tyr163–Tyr218, and Phe175–Tyr218 pairs are observed (Figure 7a and Table 2).

In summary, detailed examinations of pH-dependent structural variations showed that overall structural features of HuPrP with the fCJD-related V210I mutation are retained, while significant changes are observed in the interactions among secondary structure elements. The most prominent structural rearrangements in HuPrP(V210I) at pH 7.2, when compared to those at pH 5.5, are clustered in the $\alpha_2-\alpha_3$ interhelical region, at the interface of the $\beta_1-\alpha_1$ loop with helices α_1 and α_3, and in the $\beta_2-\alpha_2$ loop region. Our findings suggest that tertiary contacts between residues involved in these secondary structure elements are perturbed to a lesser extent in HuPrP(V210I) at pH 7.2 than at 5.5. This suggests a higher structural stability of HuPrP(V210I) under neutral-pH conditions. Therefore, we hypothesize that spontaneous misfolding of PrP^{C} in inherited prion diseases is favored under acidic-pH conditions and presumably takes place in the endosomal compartments.

AUTHOR INFORMATION

Corresponding Author

*J.P.: Slovenian NMR Centre, National Institute of Chemistry, Hajdrihova 19, SI-1000 Ljubljana, Slovenia; phone, +38614760353; fax, +38614760300; e-mail, janez.plavec@ki.si. G.L.: Laboratory of Prion Biology, Department of Neuroscience, Scuola Internazionale Superiore di Studi Avanzati (SISSA), via Bonomea 265, I-34136 Trieste, Italy; phone, +390403787715; fax, +390403787702; e-mail, giuseppe.legname@sissa.it.

Present Address

[@]Department of Chemistry, Faculty of Science, University of Zagreb, Horvatovac 102A, HR-10000 Zagreb, Croatia.

Author Contributions

I.B., G.I., and G.G. contributed equally to the work.

Funding

This research was supported by the Slovenian Research Agency (ARRS, Grant P1-0242), the EAST-NMR FP7 project (Contract 228461), the Bio-NMR FP7 project (Contract 261863), and the PRIORITY FP7 project (Contract 222887).

Notes

The authors declare no competing financial interest.

ABBREVIATIONS

NMR, nuclear magnetic resonance; 3D, three-dimensional; HSQC, heteronuclear single-quantum coherence; NOE, nuclear Overhauser enhancement; NOESY, NOE spectroscopy; PDB, Protein Data Bank; rmsd, root-mean-square deviation; TOCSY, total correlation spectroscopy.

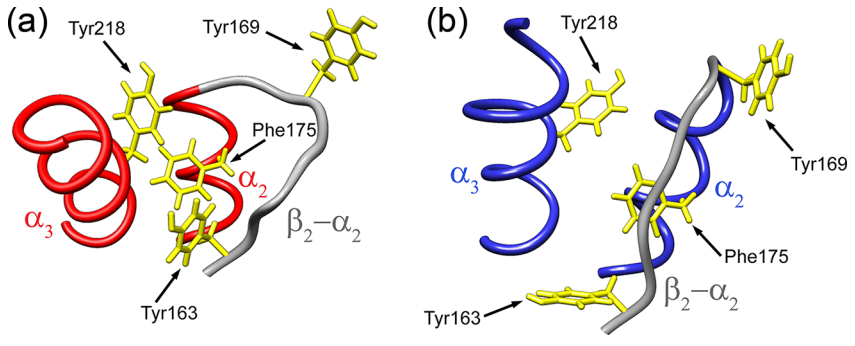

Figure 7. $\pi-\pi$ interactions at the interface of the $\beta_2-\alpha_2$ loop and the C-terminal part of helix α_3 in HuPrP(V210I) at (a) pH 7.2 and (b) pH 5.5.

dx.doi.org/10.1021/bi3009856 | *Biochemistry* 2012, 51, 7465–7474

REFERENCES

(1) Colby, D. W., and Prusiner, S. B. (2011) Prions. *Cold Spring Harbor Perspectives in Biology*, Vol. 3, Cold Spring Harbor Laboratory Press, Plainview, NY.

(2) Legname, G., Giachin, G., and Benetti, F. (2012) *Structural Studies of Prion Proteins and Prions, Non-fibrillar Amyloidogenic Protein Assemblies: Common Cytotoxins Underlying Degenerative Diseases* (Rahimi, F., and Bitan, G., Eds.) pp 289−317, Springer, Dordrecht, The Netherlands.

(3) Riek, R., Hornemann, S., Wider, G., Glockshuber, R., and Wuthrich, K. (1997) NMR characterization of the full-length recombinant murine prion protein, mPrP(23−231). *FEBS Lett. 413*, 282−288.

(4) Zahn, R., Liu, A., Luhrs, T., Riek, R., von Schroetter, C., Lopez Garcia, F., Billeter, M., Calzolai, L., Wider, G., and Wuthrich, K. (2000) NMR solution structure of the human prion protein. *Proc. Natl. Acad. Sci. U.S.A. 97*, 145−150.

(5) Taylor, D. R., and Hooper, N. M. (2006) The prion protein and lipid rafts. *Mol. Membr. Biol. 23*, 89−99.

(6) Pan, K. M., Baldwin, M., Nguyen, J., Gasset, M., Serban, A., Groth, D., Mehlhorn, I., Huang, Z., Fletterick, R. J., Cohen, F. E., et al. (1993) Conversion of α-helices into β-sheets features in the formation of the scrapie prion proteins. *Proc. Natl. Acad. Sci. U.S.A. 90*, 10962−10966.

(7) Surewicz, W. K., and Apostol, M. I. (2011) Prion protein and its conformational conversion: A structural perspective. *Top. Curr. Chem. 305*, 135−167.

(8) Aguzzi, A., and Falsig, J. (2012) Prion propagation, toxicity and degradation. *Nat. Neurosci. 15*, 936−939.

(9) Biljan, I., Giachin, G., Ilc, G., Zhukov, I., Plavec, J., and Legname, G. (2012) Structural basis for the protective effect of the human prion protein carrying the dominant-negative E219K polymorphism. *Biochem. J. 446*, 243−251.

(10) Ilc, G., Giachin, G., Jaremko, M., Jaremko, L., Benetti, F., Plavec, J., Zhukov, I., and Legname, G. (2010) NMR structure of the human prion protein with the pathological Q212P mutation reveals unique structural features. *PloS One 5*, e11715.

(11) Biljan, I., Ilc, G., Giachin, G., Raspadori, A., Zhukov, I., Plavec, J., and Legname, G. (2011) Toward the Molecular Basis of Inherited Prion Diseases: NMR Structure of the Human Prion Protein with V210I Mutation. *J. Mol. Biol. 412*, 660−673.

(12) Biasini, E., Turnbaugh, J. A., Massignan, T., Veglianese, P., Forloni, G., Bonetto, V., Chiesa, R., and Harris, D. A. (2012) The toxicity of a mutant prion protein is cell-autonomous, and can be suppressed by wild-type prion protein on adjacent cells. *PLoS One 7*, e33472.

(13) Canello, T., Friedman-Levi, Y., Mizrahi, M., Binyamin, O., Cohen, E., Frid, K., and Gabizon, R. (2012) Copper is toxic to PrP-ablated mice and exacerbates disease in a mouse model of E200K genetic prion disease. *Neurobiol. Dis. 45*, 1010−1017.

(14) Friedman-Levi, Y., Meiner, Z., Canello, T., Frid, K., Kovacs, G. G., Budka, H., Avrahami, D., and Gabizon, R. (2011) Fatal prion disease in a mouse model of genetic E200K Creutzfeldt-Jakob disease. *PLoS Pathog. 7*, e1002350.

(15) Jackson, W. S., Borkowski, A. W., Faas, H., Steele, A. D., King, O. D., Watson, N., Jasanoff, A., and Lindquist, S. (2009) Spontaneous generation of prion infectivity in fatal familial insomnia knockin mice. *Neuron 63*, 438−450.

(16) Senatore, A., Colleoni, S., Verderio, C., Restelli, E., Morini, R., Condliffe, S. B., Bertani, I., Mantovani, S., Canovi, M., Micotti, E., Forloni, G., Dolphin, A. C., Matteoli, M., Gobbi, M., and Chiesa, R. (2012) Mutant PrP suppresses glutamatergic neurotransmission in cerebellar granule neurons by impairing membrane delivery of VGCC $\alpha(2)\delta$-1 Subunit. *Neuron 74*, 300−313.

(17) Legname, G. (2012) Early structural features in mammalian prion conformation conversion. *Prion 6*, 37−39.

(18) Van der Kamp, M. W., and Daggett, V. (2009) The consequences of pathogenic mutations to the human prion protein. *Protein Eng., Des. Sel. 22*, 461−468.

(19) Van der Kamp, M. W., and Daggett, V. (2011) Molecular Dynamics as an Approach to Study Prion Protein Misfolding and the Effect of Pathogenic Mutations. *Top. Curr. Chem. 305*, 169−197.

(20) Godsave, S. F., Wille, H., Kujala, P., Latawiec, D., DeArmond, S. J., Serban, A., Prusiner, S. B., and Peters, P. J. (2008) Cryo-immunogold electron microscopy for prions: Toward identification of a conversion site. *J. Neurosci. 28*, 12489−12499.

(21) Pimpinelli, F., Lehmann, S., and Maridonneau-Parini, I. (2005) The scrapie prion protein is present in flotillin-1-positive vesicles in central- but not peripheral-derived neuronal cell lines. *Eur. J. Neurosci. 21*, 2063−2072.

(22) Mayor, S., Sabharanjak, S., and Maxfield, F. R. (1998) Cholesterol-dependent retention of GPI-anchored proteins in endosomes. *EMBO J. 17*, 4626−4638.

(23) Casey, J. R., Grinstein, S., and Orlowski, J. (2010) Sensors and regulators of intracellular pH. *Nat. Rev. Mol. Cell Biol. 11*, 50−61.

(24) Marijanovic, Z., Caputo, A., Campana, V., and Zurzolo, C. (2009) Identification of an Intracellular Site of Prion Conversion. *PLoS Pathog. 5*, e1000426.

(25) Campana, V., Sarnataro, D., and Zurzolo, C. (2005) The highways and byways of prion protein trafficking. *Trends Cell Biol. 15*, 102−111.

(26) Porto-Carreiro, I., Fevrier, B., Paquet, S., Vilette, D., and Raposo, G. (2005) Prions and exosomes: From PrPc trafficking to PrPsc propagation. *Blood Cells, Mol., Dis. 35*, 143−148.

(27) Alonso, D. O. V., deArmond, S. J., Cohen, F. E., and Daggett, V. (2001) Mapping the early steps in the pH-induced conformational conversion of the prion protein. *Proc. Natl. Acad. Sci. U.S.A. 98*, 2985−2989.

(28) DeMarco, M. L., and Daggett, V. (2007) Molecular Mechanism for Low pH Triggered Misfolding of the Human Prion Protein. *Biochemistry 46*, 3045−3054.

(29) Hornemann, S., and Glockshuber, R. (1998) A scrapie-like unfolding intermediate of the prion protein domain PrP(121−231) induced by acidic pH. *Proc. Natl. Acad. Sci. U.S.A. 95*, 6010−6014.

(30) Langella, E., Improta, R., and Barone, V. (2004) Checking the pH-Induced Conformational Transition of Prion Protein by Molecular Dynamics Simulations: Effect of Protonation of Histidine Residues. *Biophys. J. 87*, 3623−3632.

(31) Swietnicki, W., Petersen, R. B., Gambetti, P., and Surewicz, K. (1997) pH-dependent Stability and Conformation of the Recombinant Human Prion Protein PrP(90−231). *J. Biol. Chem. 272*, 27517−27520.

(32) Van der Kamp, M. W., and Daggett, V. (2010) Influence of pH on the Human Prion Protein: Insights into the Early Steps of Misfolding. *Biophys. J. 99*, 2289−2298.

(33) Calzolai, L., and Zahn, R. (2003) Influence of pH on NMR Structure and Stability of the Human Prion Protein Globular Domain. *J. Biol. Chem. 278*, 35592−35596.

(34) Pocchiari, M., Salvatore, M., Cutruzzola, F., Genuardi, M., Allocatelli, C. T., Masullo, C., Macchi, G., Alema, G., Galgani, S., Xi, Y. G., et al. (1993) A new point mutation of the prion protein gene in Creutzfeldt-Jakob disease. *Ann. Neurol. 34*, 802−807.

(35) Kovacs, G. G., Puopolo, M., Ladogana, A., Pocchiari, M., Budka, H., van Duijn, C., Collins, S. J., Boyd, A., Giulivi, A., Coulthart, M., Delasnerie-Laupretre, N., Brandel, J. P., Zerr, I., Kretzschmar, H. A., de Pedro-Cuesta, J., Calero-Lara, M., Glatzel, M., Aguzzi, A., Bishop, M., Knight, R., Belay, G., Will, R., and Mitrova, E. (2005) Genetic prion disease: The EUROCJD experience. *Hum. Genet. 118*, 166−174.

(36) Ladogana, A., Puopolo, M., Poleggi, A., Almonti, S., Mellina, V., Equestre, M., and Pocchiari, M. (2005) High incidence of genetic human transmissible spongiform encephalopathies in Italy. *Neurology 64*, 1592−1597.

(37) Delaglio, F., Grzesiek, S., Vuister, G. W., Zhu, G., Pfeifer, J., and Bax, A. (1995) NMRPipe: A multidimensional spectral processing system based on UNIX pipes. *J. Biomol. NMR 6*, 277−293.

(38) Goddard, T. D., and Kneller, D. G. (2010) *SPARKY 3*, University of California, San Francisco.

(39) Keller, R. (2004) *The Computer Aided Resonance Assignment Tutorial*, CANTINA Verlag.

(40) Guntert, P., Mumenthaler, C., and Wuthrich, K. (1997) Torsion angle dynamics for NMR structure calculation with the new program DYANA. *J. Mol. Biol. 273*, 283−298.
(41) Herrmann, T., Guntert, P., and Wuthrich, K. (2002) Protein NMR structure determination with automated NOE assignment using the new software CANDID and the torsion angle dynamics algorithm DYANA. *J. Mol. Biol. 319*, 209−227.
(42) Krieger, E., Koraimann, G., and Vriend, G. (2002) Increasing the precision of comparative models with YASARA NOVA: A self-parameterizing force field. *Proteins: Struct., Funct., Genet. 47*, 477−486.
(43) Laskowski, R. A., Rullmann, J. A. C., MacArthur, M. W., Kaptein, R., and Thornton, J. M. (1996) AQUA and PROCHECK-NMR: Programs for checking the quality of protein structures solved by NMR. *J. Biomol. NMR 8*, 477−486.
(44) Vriend, G. (1990) A molecular modelling and drug design program. *J. Mol. Graphics 9*, 52−56.
(45) Sharma, D., and Rajarathnam, K. (2000) ^{13}C NMR chemical shifts can predict disulfide bond formation. *J. Biomol. NMR 18*, 165−171.
(46) Adrover, M., Pauwels, K., Prigent, S., de Chiara, C., Xu, Z., Chapuis, C., Pastore, A., and Rezaei, H. (2010) Prion fibrillization is mediated by a native structural element that comprises helices H2 and H3. *J. Biol. Chem. 285*, 21004−21012.
(47) Van der Kamp, M. W., and Daggett, V. (2010) Pathogenic mutations in the hydrophobic core of the human prion protein can promote structural instability and misfolding. *J. Mol. Biol. 404*, 732−748.
(48) Prusiner, S. B. (2012) A unifying role for prions in neurodegenerative disorders. *Science 336*, 1511−1513.
(49) Eghiaian, F., Daubenfeld, T., Quenet, Y., Van Audenhaege, M., Bouin, A., Van der Rest, G., Grosclaude, J., and Rezaei, H. (2007) Diversity in prion protein oligomerization pathways results from domain expansion as revealed by hydrogen/deuterium exchange and disulfide linkage. *Proc. Natl. Acad. Sci. U.S.A. 104*, 7414−7419.
(50) Watzlawik, J., Skora, L., Frense, D., Griesinger, C., Zweckstetter, M., Schulz-Schaeffer, W. J., and Kramer, M. L. (2006) Prion protein helix 1 promotes aggregation but is not converted into β-sheet. *J. Biol. Chem. 281*, 30242−30250.
(51) Langella, E., Improta, R., Crescenzi, O., and Barone, V. (2006) Assessing the acid-base and conformational properties of histidine residues in human prion protein (125−228) by means of pK_a calculations and molecular dynamics simulations. *Proteins 64*, 167−177.
(52) Dolinsky, T. J., Czodrowski, P., Li, H., Nielsen, J. E., Jensen, J. H., Klebe, G., and Baker, N. A. (2007) PDB2PQR: Expanding and upgrading automated preparation of biomolecular structures for molecular simulations. *Nucleic Acids Res. 35*, W522−W525.
(53) Baker, N. A., Sept, D., Joseph, S., Holst, M. J., and McCammon, J. A. (2001) Electrostatics of nanosystems: Application to microtubules and the ribosome. *Proc. Natl. Acad. Sci. U.S.A. 98*, 10037−10041.
(54) Li, H., Robertson, A. D., and Jensen, J. H. (2005) Very fast empirical prediction and rationalization of protein pKa values. *Proteins 61*, 704−721.